

# High-Yield production of water-soluble MoS<sub>2</sub> quantum dots for Fe<sup>3+</sup> detection and cell imaging

Benhua Xu,<sup>a,d</sup> Zhiqi Zhang,<sup>a</sup> Li Wang,<sup>c</sup> Rui Yuan,<sup>a</sup> Zhenghua Ju,<sup>d</sup> Peng Zhang,<sup>b,\*</sup>  
Weisheng Liu<sup>d,\*</sup>

- a. Chemical Engineering College, Qinghai University, Xining 810016, China
- b. Qinghai Provincial Key Laboratory of New Light Alloys, Qinghai Provincial Engineering Research Center of High-Performance Light Metal Alloys and Forming, Qinghai University, Xining 810016, P. R China
- c. College of Chemistry and Chemical Engineering, Xi'an Shiyou University, Xi'an 710065, P. R. China
- d. Key Laboratory of Nonferrous Metals Chemistry and Resources Utilization of Gansu Province and State Key Laboratory of Applied Organic Chemistry, College of Chemistry and Chemical Engineering, Lanzhou University, Lanzhou 730000, P. R. China.

\*Correspondence should be addressed.

E-mail: zhangpeng@qhu.edu.cn and zhangp\_13@163.com (Peng Zhang)

E-mail: liuws@lzu.edu.cn.(Weisheng Liu)

## Abstract

Uniform water soluble MoS<sub>2</sub> quantum dots (WS-MSQDs) are synthesized via a sequential combination of sintering/etching/exfoliation method and solvothermal route. The obtained WS-MSQDs with average size of approximately 3.4 nm exhibit sufficient water solubility and remarkable fluorescence properties. The WS-MSQDs have been utilized as a probe for detection of Fe<sup>3+</sup> ions with high selectivity and specificity. Furthermore, the WS-MSQDs exhibit high fluorescence stability under different conditions. Finally, the WS-MSQDs are successfully applied for the fluorescence imaging of Fe<sup>3+</sup> in living cells, which exhibited practical potential for biomedical applications.

Key words: Water-soluble MoS<sub>2</sub> quantum dots, Fluorescent probe, Fe<sup>3+</sup> ion sensor, Living cells

## 1. Introduction

Two-dimensional (2D) transition-metal dichalcogenides (TMDCs) have drawn tremendous attention and shown great promise for various applications in energy storage and conversion, electronic devices and biomedicine[1-3]. When the lateral dimensions of 2D TMDCs are reduced into quantum dots, unique optical and electronic properties are introduced into TMDCs quantum dots owing to quantum confinement and edge effects[4]. Among the large family of TMDCs quantum dots, Molybdenum disulfide ( $\text{MoS}_2$ ) quantum dots (MSQDs) are the most representative and have shown remarkable applications in biology, catalyzing, electrochemical and optoelectronic devices[5].

In widely applications, especially biology, MSQDs need to possess good water-solubility, fine photo-stability, low cytotoxicity and excellent biocompatibility[6]. The above advantages promote their widespread applications in fluorescence sensing[7, 8] and bioimaging[9, 10] etc. Wu et al. have obtained MSQDs by a top-down method and the MSQDs with strong fluorescence, good cell permeability and low cytotoxicity are used as probes for in vitro imaging[11]. Recently, luminescent MS nanosheets based fluorescent sensors are applied to detect metal ions ( $\text{Fe}^{2+}$ ,  $\text{Hg}^{2+}$ )[12]. Hence, MSQDs have potential to be novel fluorescent probes for metal ions. Among the metal ions,  $\text{Fe}^{3+}$  plays crucial roles in the growth and development of biological systems[13-16] and amounts of analysis strategies have been developed to qualitatively and quantitatively detect  $\text{Fe}^{3+}$  ion in biological systems for the early identification and diagnosis of these diseases[17-19]. In past two decades, fluorescence spectrometry is gradually drawing considerable attention to directly detect  $\text{Fe}^{3+}$  because of its advantages of high sensitivity, excellent

reproducibility, rapid response and good selectivity[20-24]. Up to date, a series of quantum dots-based fluorescent  $\text{Fe}^{3+}$  probes have been fabricated. Among them, MSQDs-based nanoprobe are representative. Ruan et al. synthesized high water-solubility MSQDs (WS-MSQDs) by the combination the ethylenediamine-assisted exfoliation and hydrothermal process[25]. Yu et al. prepared MSQDs from one-step hydrothermal exfoliation procedure[26]. These obtained MSQDs exhibit excellent fluorescence and are effective fluorescent probes for detecting  $\text{Fe}^{3+}$  ions with excellent sensitivity, selectivity, and fast response. However, these synthesis methods still suffer from low yield of the WS-MSQDs. Hence, it is necessary to develop a simple approach for mass production of WS-MSQDs for fully developing their properties.

In past few years, a variety of strategies have been employed for synthesizing WS-MSQDs, including top-down and bottom-up methods. For top-down approaches, the lateral size of layered MS is reduced through physical or chemical methods, including sequential combination of salt-assisted ball-milling and sonication-assisted solvent exfoliation method[27], electrochemical approach[28], ultrafast laser ablation[29], combination of grinding/hydrothermal process and sonication[30], liquid exfoliation[31] and sodium-ion intercalation-assisted approach[32] etc. In these methods, the in-plane chemical bonds of bulk MS are broken by external forces or chemical cutting processes and then the weak interlayer van der Waals interactions are broken by liquid exfoliation. So these approaches suffer from time-consuming, rigorous conditions, tedious post-treatment and low yield of the QDs. For bottom-up approaches, the WS-MSQDs are synthesized by hydrothermal and solvothermal method[33-35] using different molybdenum and sulfur sources.

However these methods also suffer from cumbersome post-treatment. The above drawbacks impede their practical applications. In our previous work, we developed an efficient bottom-up strategy for high-yield production of WS-MSQDs by a sintering/etching/exfoliation approach and the yield of WS-MSQDs is over 30%[36]. But the water solubility of obtained MSQDs is poor. This disadvantage prejudices their biology applications.

In this paper, we report a simple and efficient method for large scale production of WS-MSQDs by a bottom up strategy. The obtained WS-MSQDs exhibit sufficient water solubility and remarkable fluorescence properties, which have been utilized as a probe for detection of  $\text{Fe}^{3+}$  ions with high selectivity and specificity. Furthermore, the WS-MSQDs are used for the fluorescence imaging of  $\text{Fe}^{3+}$  in living cells successfully.

## **2. Experimental Section**

### **2.1 Materials and Apparatus**

All reagents or solvents were purchased from commercial providers and used without further purification. The transmission electron microscope (TEM) images were obtained from FEI Tecnai F30 microscope. The atomic force microscope (AFM) was performed on an Asylum Research MFP-3D instrument. The crystal structure properties of samples were characterized by an X-ray diffraction instrument (XRD, Phillips X'pert Pro). Raman spectra of the samples were performed on a micro-Raman spectroscopy (JY-HR800). The X-ray photoelectron spectroscopy (XPS) spectra were measured by HORIBA Jobin Yvon LabRAM-HR800 microscope. The UV-vis spectra were recorded with an Agilent Cary 5000 spectrophotometer. The luminescence spectra were

recorded using a Hitachi F-7000 spectrophotometer. All pH measurements were made with a pH-10C digital pH meter.

## 2.2 Synthesis of WS-MSQDs

The WS-MSQDs were synthesised through the methods describing in our previous paper with minor modification[36]. In order to improve the water solubility of obtained MSQDs, the resulted powder after etching process need a solvothermal treatment. Briefly, 50 mg resulted powder was dispersed into 200 mL N, N-dimethylformamide (DMF). After sonicating in an ice bath for 3 h, the dispersion was kept stirring for 4 h at 140 °C. Afterwards, the stabilized deep yellow suspension containing amount of WS-MSQDs was obtained by centrifuging at 4000 rpm for 15 min. The supernatant was evaporated under vacuum at 80 °C and then dispersed in deionized water. The yield of water soluble WS-MSQDs is about 30 wt %.

## 2.3 Photoluminescence measurement

All the fluorescence measurements were performed in HEPES (10 mM, pH 7.2) buffer solution at room temperature. Stock solution of metal ions including  $\text{Fe}^{3+}$ ,  $\text{Ag}^+$ ,  $\text{Al}^{3+}$ ,  $\text{Ba}^{2+}$ ,  $\text{Ca}^{2+}$ ,  $\text{Cd}^{2+}$ ,  $\text{Co}^{2+}$ ,  $\text{Cr}^{3+}$ ,  $\text{Ga}^{3+}$ ,  $\text{Hg}^{2+}$ ,  $\text{K}^+$ ,  $\text{Li}^+$ ,  $\text{Mg}^{2+}$ ,  $\text{Mn}^{2+}$ ,  $\text{Na}^+$ ,  $\text{Ni}^{2+}$ ,  $\text{Pb}^{2+}$  and  $\text{Zn}^{2+}$  in acetonitrile were prepared with an concentration of  $10^{-1}$  M using their perchlorates, and stock solution of WS-MSQDs (100  $\mu\text{g/mL}$ ) in deionized water was prepared. In a typical assay, 200  $\mu\text{L}$  WS-MSQDs stock solution was diluted in 1800  $\mu\text{L}$  HEPES buffer solution at a final concentration of 10  $\mu\text{g/mL}$ . For cation competitiveness study, 10  $\mu\text{L}$  of these metal ions were added into the above solution at a final concentration of 500  $\mu\text{M}$ .

## 2.4 Cell culture

BHK cells were seeded to the 12-well plates and cultured in culture media (Dulbecco's Modified Eagle Medium) subjoined with 10% FBS (fetal bovine serum) at 37 °C in a humidified incubator containing 5%  $\text{CO}_2$ . After 24 h, the

cells incubated with 20  $\mu\text{g/mL}$  WS-MSQDs for 1 h and then they were incubated with (100  $\mu\text{M}$ )  $\text{Fe}(\text{ClO}_4)_3$  for another 1 h. For the control experiment, BHK cells incubated only with 20  $\mu\text{g/mL}$  WS-MSQDs for 1 h under the same conditions. Before imaging measurement, the cells were rinsed three times with phosphate buffered saline.

### **3. Results and discussion**

#### **3.1. Characterizations of MSQDs**

$\text{MoCl}_5$  (0.5 g) and thiourea (1 g) are used as molybdenum and sulfur source to synthesize WS-MSQDs via sintering/etching/exfoliation process describing in our previous paper. However, the obtained MSQDs exhibit poor water solubility. For improving water solubility of MSQDs, the obtained MS nanoplates composing of stripe-like grains were subjected to a solvothermal treatment. Finally, WS-MSQDs were obtained by liquid exfoliating of MS nanoplates and centrifugation. The production yield of WS-MSQDs exceeds 30 wt %, indicating the significant competitiveness of the synthetic method we proposed toward mass production of the WS-MSQDs.

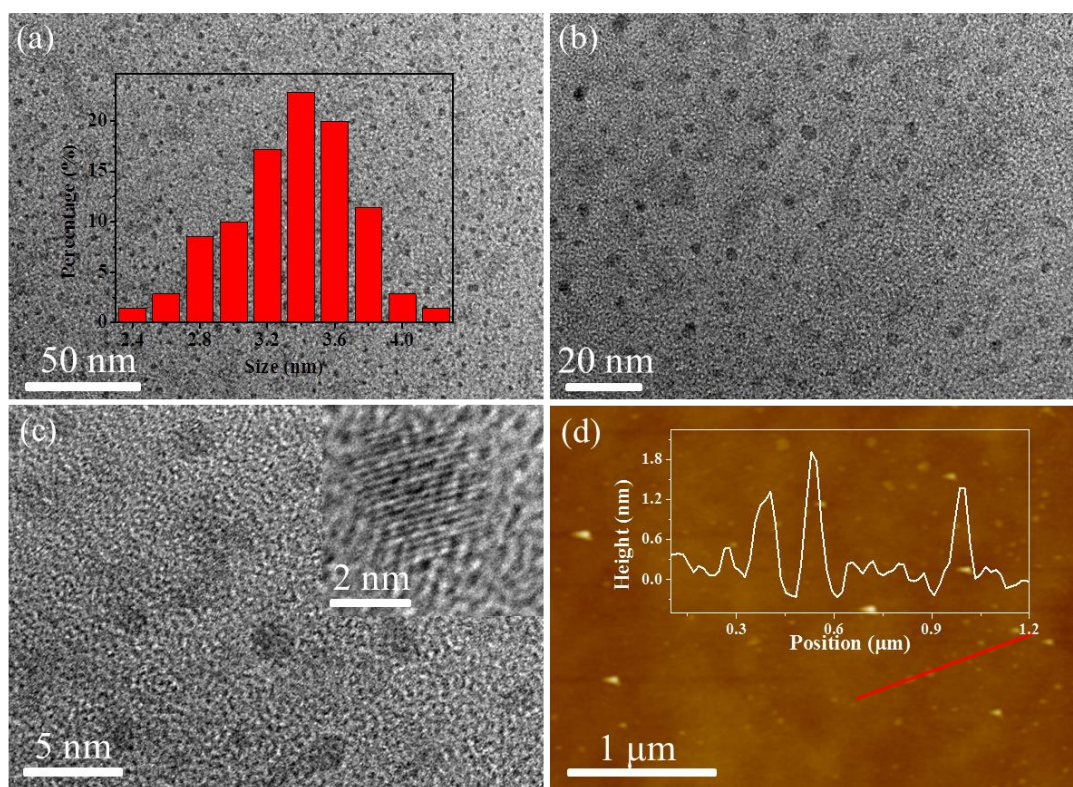


Fig. 1. Morphology characterization of WS-MSQDs. (a-c) TEM images of WS-MSQDs. Inset of (a, c): the size distributions and HRTEM pattern of the WS-MSQDs. (d) AFM image of the WS-MSQDs. Inset of (d): height profiles along the red lines in (d).

The WS-MSQDs were characterized by transmission electron microscopy (TEM). TEM images (Fig. 1a and 1b) exhibit that the WS-MSQDs are uniformly distributed without aggregation and the average size is 3.4 nm. Furthermore, the high-resolution TEM (HRTEM) images (Fig. 1c) indicate the highly crystalline structure of the WS-MSQDs. The morphology and thickness of WS-MSQDs were investigated by atomic force microscope (AFM), which confirmed the height of the WS-MSQDs varies from 0.6 to 1.8 nm. The energy-dispersive X-ray spectrometry (EDX) spectra, as shown in Fig. 2a, indicate that only the elements of Mo and S present in WS-MSQDs. The element Cu comes from the copper grid for TEM measurement. Furthermore, the chemical state and surface composition of WS-MSQDs were investigated by X-ray photoelectron spectroscopy (XPS) measurements (Fig. 2b). As shown

in Fig. 2b, no peak for Si was detected, indicating that nano-SiO<sub>2</sub> in the product were removed completely. Fig. 2c and d depict the high-resolution XPS of the WS-MSQDs in the Mo 3d and S 2p. As shown in Fig. 2c, the two main peaks at 232.1 and 228.8 eV corresponded to Mo<sup>4+</sup> 3d<sub>3/2</sub> and Mo<sup>4+</sup> 3d<sub>5/2</sub>, respectively, and the peak at 225.9 eV is S 2s. As shown in Fig. 2d, two peaks at 161.7 and 162.8 eV corresponded to S 2p<sub>3/2</sub> and S 2p<sub>1/2</sub>, respectively[37]. These results indicate that the obtained WS-MSQDs are trigonal prismatic (2H) phase.

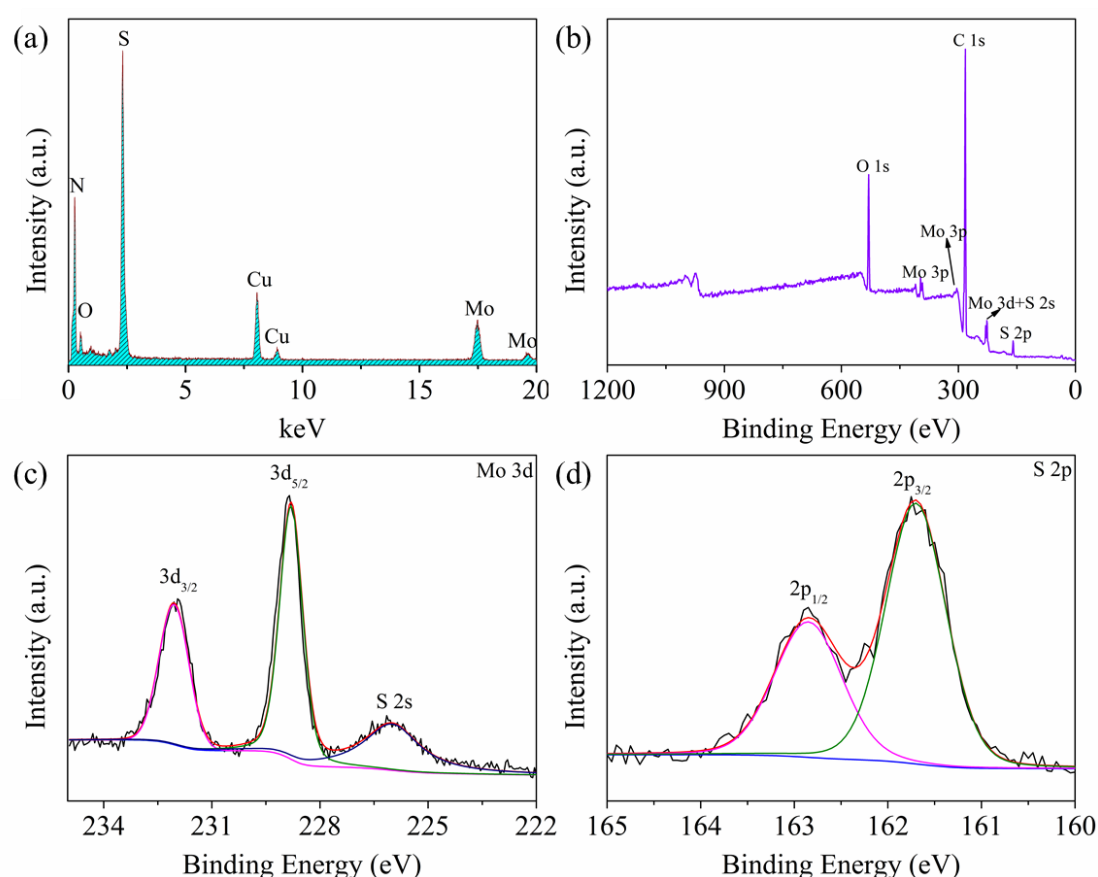


Fig. 2. (a) EDX spectrum of the WS-MSQDs. (b) XPS image of the WS-MSQDs. The high-resolution XPS spectra of (c) Mo 3d and (d) S 2p.

The phase identity of the WS-MSQDs was confirmed by Powder X-ray diffraction (XRD) and Raman spectroscopy measurements. Fig. 3a depicts the XRD data for the WS-MSQDs and MS nanosheets is used as a reference. It depicts that only two weak diffraction peaks are detected at 32.82 ° and 58.42 °

for WS-MSQDs, and the most of other peaks are disappearance. It demonstrates the formation of mono- or few-layered WS-MSQDs. Fig. 3b shows that the Raman spectra for MS nanosheets presents two distinct peaks at  $379.5\text{ cm}^{-1}$  and  $403.4\text{ cm}^{-1}$  for the  $E_{2g}^1$  and  $A_{1g}^1$  vibrational modes, respectively[38]. The  $E_{2g}^1$  mode of the monolayer WS-MSQDs is red-shifted compared to that of MS nanosheets, which is identical with previous report[39].

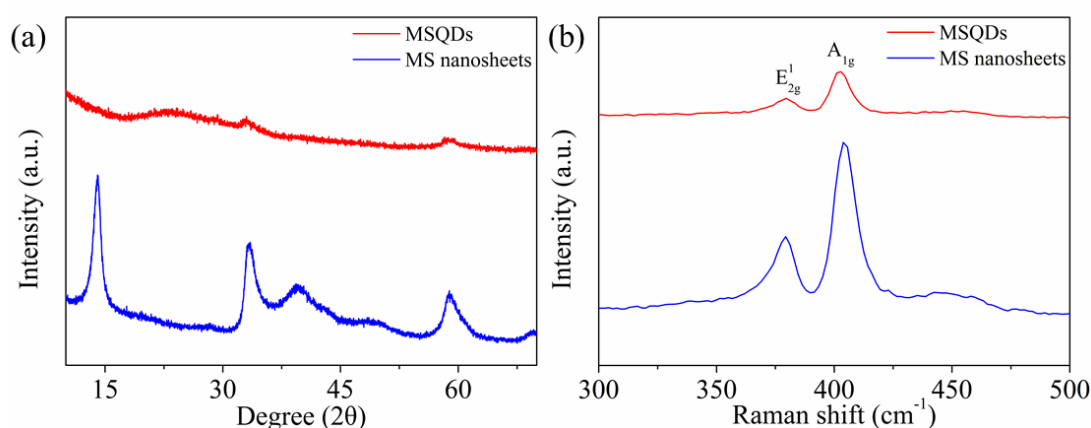


Fig. 3. (a) XRD patterns and (b) Raman spectra of the MS nanosheets and WS-MSQDs.

### 3.2. Optical Properties of MSQDs

The optical properties of the WS-MSQDs were explored in HEPES (10 mM, pH 7.2) buffer solution. The UV-vis absorption spectra show an absorption peak at 295 nm, which corresponds to the excitonic feature of WS-MSQDs, presented in Fig. 4a. The WS-MSQDs emit fluorescence at 425nm upon the excitation of 340 nm with a quantum yield of 5.9%. Fig. 4b shows the fluorescence emission spectra of the WS-MSQDs excited by the light with different wavelengths. From it, we can see the fluorescence emission of WS-MSQDs exhibited an excitation-dependent behaviour with the excitation wavelength change from 270 to 400 nm. This photoluminescence behavior is analogous to the previous report[39], which is generated from the high homogeneity and good water solubility of the WS-MSQDs.

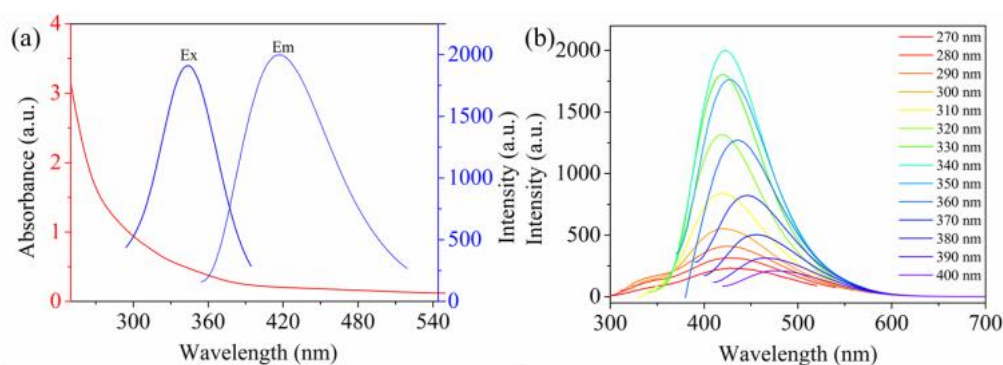


Fig. 4. (a) UV-vis absorption and fluorescence emission spectrum of WS-MSQDs. (b) Fluorescence emission spectra of WS-MSQDs at different excitation wavelength.

### 3.3. Effects of the pH

The stability of the fluorescence for WS-MSQDs under different conditions was also explored. As shown in Fig. 5a, the fluorescence intensity of WS-MSQDs is found to be independent of pH over a wide range (2.5-11.0), which indicates the influence of pH on the fluorescence of WS-MSQDs is negligible. Furthermore, the fluorescence intensity of WS-MSQDs has no significant decline under continuous irradiating at 340 nm for 30 min (Fig. 5b), suggesting WS-MSQDs possesses excellent photostability. Therefore, it is demonstrated that the fluorescence of WS-MSQDs is stable fairly under different conditions and has the potential for biological applications.

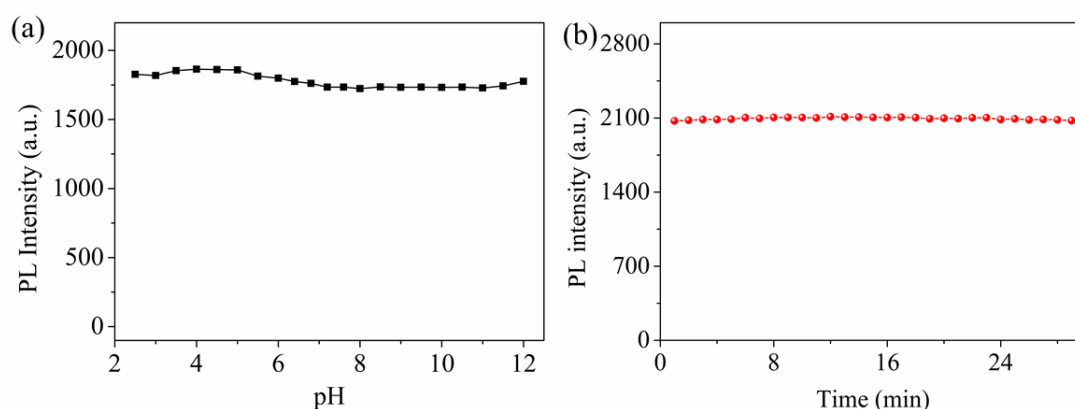


Fig. 5. The photostability of WS-MSQDs (a) Fluorescence stability studies of WS-MSQDs in different pH solutions. (b) Fluorescence intensity of WS-MSQDs under excitation at 340 nm for 30 min.

### 3.4. Detection of $\text{Fe}^{3+}$ Ions and Selectivity Measurements.

To evaluate the recognition capability of WS-MSQDs towards  $\text{Fe}^{3+}$  ions over other metal ions (such as  $\text{Ag}^+$ ,  $\text{Al}^{3+}$ ,  $\text{Ba}^{2+}$ ,  $\text{Ca}^{2+}$ ,  $\text{Cd}^{2+}$ ,  $\text{Co}^{2+}$ ,  $\text{Cr}^{3+}$ ,  $\text{Ga}^{3+}$ ,  $\text{Hg}^{2+}$ ,  $\text{K}^+$ ,  $\text{Li}^+$ ,  $\text{Mg}^{2+}$ ,  $\text{Mn}^{2+}$ ,  $\text{Na}^+$ ,  $\text{Ni}^{2+}$ ,  $\text{Pb}^{2+}$  and  $\text{Zn}^{2+}$ ), selectivity experiment was also carried out. As shown in Fig. 6a, only the addition of  $\text{Fe}^{3+}$  results significant quenching effect on the fluorescence of WS-MSQDs, whereas no obvious changes are observed upon the addition of other metal ions under the same conditions, which indicating the high selectivity of WS-MSQDs for  $\text{Fe}^{3+}$  in aqueous solutions and potential as an effective fluorescence probe for  $\text{Fe}^{3+}$  detection. Furthermore, the cation-competitive experiments were conducted in the presence  $\text{Fe}^{3+}$  ions mixed with different metal ions, shown in Fig. 6b. As a result, the fluorescence intensity has little change under the condition of these ions coexistence, suggesting the competing ions have tiny influence on the fluorescence intensity of WS-MSQDs.

Then, the sensing performance of WS-MSQDs towards  $\text{Fe}^{3+}$  was investigated systematically in HEPES (10 mM, pH 7.2) buffer solution. The fluorescence titration spectra of  $\text{Fe}^{3+}$  to WS-MSQDs are displayed in Fig. 6c. Upon addition of different concentrations of  $\text{Fe}^{3+}$  ions, the fluorescence intensity of the WS-MSQDs at 425nm decreases gradually linearly. From the linear equation (Fig. 6d), the detection limit (LOD) for  $\text{Fe}^{3+}$  ions was measured to be 2.03  $\mu\text{M}$  ( $3\sigma$  per slope) ( $R^2 = 0.9904$ ), which met the limit of  $\text{Fe}^{3+}$  in drinking water (5.357  $\mu\text{M}$ ) set by U. S. Environmental Protection Agency[40]. Therefore, WS-MSQDs could be served as a fluorescence turn-off probe for quantitative detection of  $\text{Fe}^{3+}$  ions.

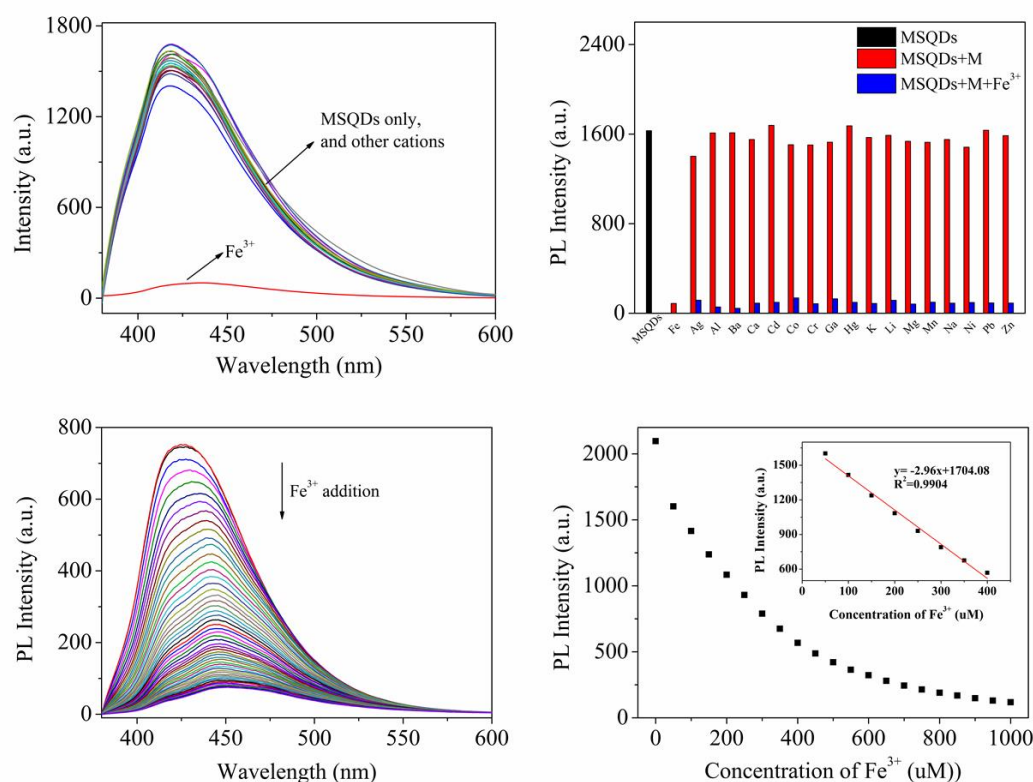


Fig. 6. (a) Fluorescence spectra of WS-MSQDs upon addition of various metal ions ( $\text{Fe}^{3+}$ ,  $\text{Ag}^+$ ,  $\text{Al}^{3+}$ ,  $\text{Ba}^{2+}$ ,  $\text{Ca}^{2+}$ ,  $\text{Cd}^{2+}$ ,  $\text{Co}^{2+}$ ,  $\text{Cr}^{3+}$ ,  $\text{Ga}^{3+}$ ,  $\text{Hg}^{2+}$ ,  $\text{K}^+$ ,  $\text{Li}^+$ ,  $\text{Mg}^{2+}$ ,  $\text{Mn}^{2+}$ ,  $\text{Na}^+$ ,  $\text{Ni}^{2+}$ ,  $\text{Pb}^{2+}$  and  $\text{Zn}^{2+}$ ). (b) Relative fluorescence intensities of WS-MSQDs at 425 nm. (black bars: WS-MSQDs; red bars: WS-MSQDs with other metals; blue bars: WS-MSQDs with other metals ions and  $\text{Fe}^{3+}$  ions). (c) Fluorescence spectra of WS-MSQDs in the presence of different concentration of  $\text{Fe}^{3+}$  ions. (d) Fluorescence intensity of WS-MSQDs versus increasing concentrations of  $\text{Fe}^{3+}$  ions. Inset of (d): The linear changes of fluorescence intensity of WS-MSQDs at 425 nm upon titration with  $\text{Fe}^{3+}$  ions. All spectra were acquired in HEPES (10 mM, pH 7.2) buffer solution at room temperature. [WS-MSQDs] = 10  $\mu\text{g/mL}$ ,  $\lambda_{\text{ex}}$  = 340 nm, Slit: 5.0 nm/5.0 nm.

### 3.5. Fluorescence imaging

In addition, considering the positive results in vitro, the fluorescence imaging of WS-MSQDs for  $\text{Fe}^{3+}$  in living cells was studied. As shown in Fig. 7a, An intense intracellular blue fluorescence could be seen when BHK cells incubated with WS-MSQDs (20  $\mu\text{g/mL}$ ) for 1 h at 37  $^{\circ}\text{C}$ , which implying that WS-MSQDs possessed good cell membrane permeability. However, the cells treated with WS-MSQDs 20  $\mu\text{g/mL}$  were further incubated with  $\text{Fe}^{3+}$  (100  $\mu\text{M}$ )

for another 1 h (Fig. 7b), an obvious fluorescence decrease was observed, which was in agreement with the  $\text{Fe}^{3+}$  induced fluorescence response. Taken together, WS-MSQDs was biocompatible and suitable for imaging of  $\text{Fe}^{3+}$  in living cells.

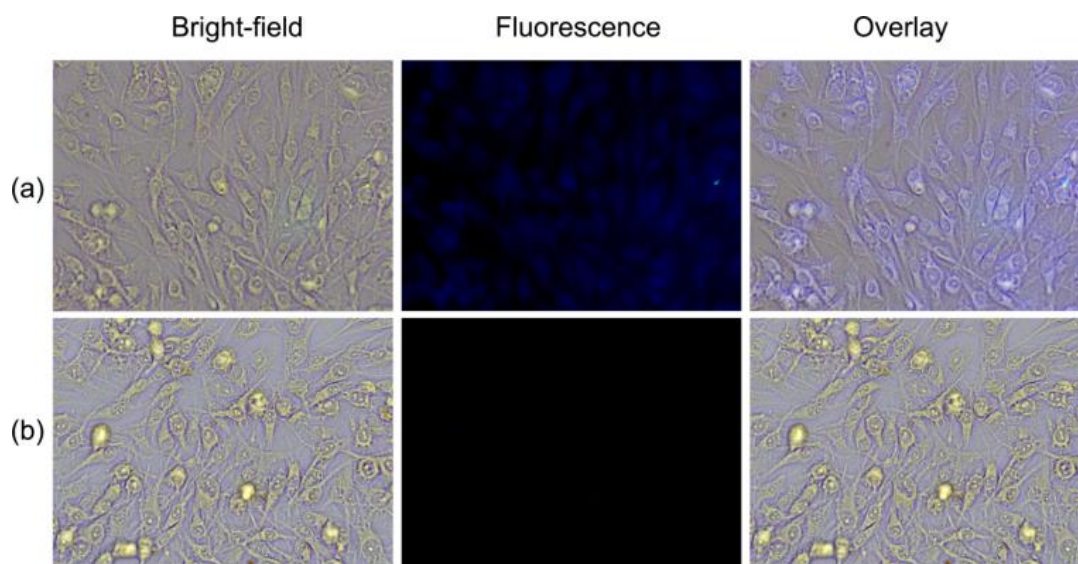


Fig. 7. Bright-field and fluorescence images of BHK cells. (a) BHK cells were incubated with WS-MSQDs (20  $\mu\text{g/mL}$ ) for 1 h. (b) BHK cells were incubated with WS-MSQDs (20  $\mu\text{g/mL}$ ) for 1 h and then further incubated with  $\text{Fe}^{3+}$  (100  $\mu\text{M}$ ) for 1 h.

#### 4. Conclusion

In summary, mass production of WS-MSQDs was achieved via a sequential combination of sintering/etching/exfoliation method and solvothermal route. With such a strategy, uniform WS-MSQDs were produced with a high yield more than 30 wt %, indicating the significant competitiveness of the synthetic method we proposed toward mass production of the WS-MSQDs. The obtained WS-MSQDs with average size of 3.4 nm display sufficient water solubility and remarkable fluorescence properties. Furthermore, the WS-MSQDs have been utilized as a probe for the selective and sensitive detection of  $\text{Fe}^{3+}$  ions. The WS-MSQDs exhibit highly fluorescence stability under a wide range of pH and continuous irradiation. Finally, the WS-MSQDs were used for the fluorescence

imaging of  $\text{Fe}^{3+}$  in living cells, which exhibited practical potential for various bio-applications.

**Author Contributions:** Benhua Xu: Conceptualization; Investigation; Writing-Original Draft. Zhiqi Zhang: Investigation; Writing-Original Draft. Li Wang: Conceptualization; Resources. Rui Yuan: Formal analysis. Zhenghua Ju: Formal analysis. Peng Zhang: Funding acquisition; Formal analysis. Weisheng Liu: Funding acquisition; Resources.

**Funding:** This work was funded by the Natural Science Foundation of Qinghai Province (2019-ZJ-945Q), National Natural Science Foundation of China (51902171) and Thousand Talents Program of Qinghai Province.

**Acknowledgements:** Supported by the National Natural Science Foundation of China.

**Conflicts of interest:** The authors declare no conflict of interest.

## References

- 1 Mao, S.; Chang, J.; Pu, H.; Lu, G.; He, Q.; Zhang, H.; Chen, J. Two-dimensional nanomaterial-based field-effect transistors for chemical and biological sensing. *Chem. Soc. Rev.* **2017**, 46, 6872-6904.
- 2 Tan, C.; Zhang, H. Two-dimensional transition metal dichalcogenide nanosheet-based composites. *Chem. Soc. Rev.* **2015**, 44, 2713-2731.
- 3 Tan, C.; Cao, X.; Wu, X.; He, Q.; Yang, J.; Zhang, X.; Chen, J.; Zhao, W.; Han, S.; Nam, G.; Sindoro, M.; Zhang, H. Recent advances in ultrathin two-dimensional nanomaterials. *Chem. Rev.* **2017**, 117, 6225-6331.
- 4 Wang, X.; Sun, G.; Li, N.; Chen, P. Quantum dots derived from two-dimensional materials and their applications for catalysis and energy. *Chem. Soc. Rev.* **2016**, 45, 2239-2262.

- 5 Sabari Arul, N.; Nithya, V. D. Molybdenum disulfide quantum dots: synthesis and applications. *RSC adv.* **2016**, 6, 65670-65682.
- 6 Guo, Y.; Li, J. MoS<sub>2</sub> quantum dots: Synthesis, properties and biological applications. *Mater. Sci. Eng. C* **2020**, 109, 110511.
- 7 Gu, W.; Yan, Y.; Zhang, C.; Ding, C.; Xian, Y. One-step synthesis of water-soluble MoS<sub>2</sub> quantum dots via a hydrothermal method as a fluorescent probe for hyaluronidase detection. *ACS Appl. Mater. Interfaces.* **2016**, 8, 11272-11279.
- 8 Kim, M.; Jeon, S.; Kang, T. W.; Ju, J.; Yim, D.; Kim, H.; Park, J. H.; Kim, J. 2H-WS<sub>2</sub> Quantum dots produced by modulating the dimension and phase of 1T-nanosheets for antibody-free optical sensing of neurotransmitters. *ACS Appl. Mater. Interfaces.* **2017**, 9, 12316-12323.
- 9 Wang, Y.; Ni, Y. Molybdenum disulfide quantum dots as a photoluminescence sensing platform for 2, 4, 6-trinitrophenol detection. *Anal. Chem.* **2014**, 86, 7463-7470.
- 10 Wang, X.; Wu, Q.; Jiang, K.; Wang, C.; Zhang, C. One-step synthesis of water-soluble and highly fluorescent MoS<sub>2</sub> quantum dots for detection of hydrogen peroxide and glucose. *Sensor. Actuat. B-Chem.* **2017**, 252, 183-190.
- 11 Xu, S.; Li, D.; Wu, P. One-pot, facile, and versatile synthesis of monolayer MoS<sub>2</sub>/WS<sub>2</sub> quantum dots as bioimaging probes and efficient electrocatalysts for hydrogen evolution reaction. *Adv. Funct. Mater.* **2015**, 25, 1127-1136.
- 12 Wang, Y.; Hu, J.; Zhuang, Q.; Ni, Y. Enhancing sensitivity and selectivity in a label-free colorimetric sensor for detection of iron (II) ions with luminescent molybdenum disulfide nanosheet-based peroxidase mimetics. *Biosens. Bioelectron.* **2016**, 80, 111-117.
- 13 Wu, J. S.; Liu, W. M.; Ge, J. C.; Zhang, H. Y.; Wang, P. F. New sensing mechanisms for design of fluorescent chemosensors emerging in recent years. *Chem. Soc. Rev.* **2011**, 40, 3483-3495.
- 14 Sandroni, M.; Favereau, L.; Planchat, A.; Akdas-Kilig, H.; Szuwarski, N.; Pellegrin, Y.; Blart, E.; Bozec, H. L.; Boujtita, M.; Odobel, F. Heteroleptic copper(I)-polypyridine complexes as efficient sensitizers for dye sensitized solar cells. *J. Mater. Chem. A* **2014**, 2, 9944-9947.
- 15 Yang, M. Y.; Li, J.; Chen, P. R. Transition metal-mediated bioorthogonal protein chemistry in living cells. *Chem. Soc. Rev.* **2014**, 43, 6511-6526.

- 16 Rouault, T. A. The role of iron regulatory proteins in mammalian iron homeostasis and disease. *Nat. Chem. Biol.* **2006**, 2, 406.
- 17 Li, S.; Li, Y.; Cao, J.; Zhu, J.; Fan, L.; Li, X. Sulfur-doped graphene quantum dots as a novel fluorescent probe for highly selective and sensitive detection of  $\text{Fe}^{3+}$ . *Anal. Chem.* **2014**, 86, 10201-10207.
- 18 Hu, X. P.; Pan, D. W.; Lin, M. Y.; Han, H. T.; Li, F. Graphene oxide-assisted synthesis of bismuth nanosheets for catalytic stripping voltammetric determination of iron in coastal waters. *Microchim. Acta.* **2016**, 183, 855-861.
- 19 Wolle, M. M.; Fahrenholz, T.; Rahman, G. M. M.; Pamuku, M.; Kingston, H. M.; Browne, D. Method development for the redox speciation analysis of iron by ion chromatography-inductively coupled plasma mass spectrometry and carryover assessment using isotopically labeled analyte analogues. *J. Chromatogr. A* **2014**, 1347, 96-103.
- 20 Picard, M.; Thakur, S.; Misra, M.; Mohanty, A. K. Miscanthus grass-derived carbon dots to selectively detect  $\text{Fe}^{3+}$  ions. *RSC adv.* **2019**, 9, 8628-8637.
- 21 Li, K. B.; Zang, Y.; Wang, H.; Li, J.; Chen, G. R.; James, T. D.; He, X. P.; Tian, H. Hepatoma-selective imaging of heavy metal ions using a 'clicked' galactosylrhodamine probe. *Chem. Commun.* **2014**, 50, 11735-11737.
- 22 Chen, X. Q.; Tian, X. Z.; Shin, I.; Yoon, J. Y. Fluorescent and luminescent probes for detection of reactive oxygen and nitrogen species. *Chem. Soc. Rev.* **2011**, 40, 4783-4804.
- 23 Wang, F.; Wang, L.; Chen, X. Q.; Yoon, J. Y. Recent progress in the development of fluorometric and colorimetric chemosensors for detection of cyanide ions. *Chem. Soc. Rev.* **2014**, 43, 4312-4324.
- 24 Sarkar, S.; Chatti, M.; Adusumalli, V. N.; Mahalingam, V. Highly selective and sensitive detection of  $\text{Cu}^{2+}$  ions using Ce(III)/Tb(III)-doped  $\text{SrF}_2$  nanocrystals as fluorescent probe. *ACS Appl. Mater. Interfaces* **2015**, 7, 25702-25708.
- 25 Ruan, L.; Zhao, Y.; Chen, Z.; Zeng, W.; Wang, S.; Liang, D.; Zhao, J. Ethylenediamine-assisted hydrothermal method to fabricate  $\text{MoS}_2$  quantum dots in aqueous solution as a fluorescent probe for  $\text{Fe}^{3+}$  ion detection. *Appl. Surf. Sci.* **2020**, 528, 146811.

- 26 Ma, J.; Yu, H.; Jiang, X.; Luo, Z.; Zheng, Y. High sensitivity label-free detection of  $\text{Fe}^{3+}$  ion in aqueous solution using fluorescent  $\text{MoS}_2$  quantum dots. *Sensors. Actuat. B-Chem.* **2019**, 281, 989-997.
- 27 Han, C.; Zhang, Y.; Gao, P.; Chen, S.; Liu, X.; Mi, Y.; Zhang, J.; Ma, Y.; Jiang, W.; Chang, J. High-yield production of  $\text{MoS}_2$  and  $\text{WS}_2$  quantum sheets from their bulk materials. *Nano Lett.* **2017**, 17, 7767-7772.
- 28 Gopalakrishnan, D.; Damien, D.; Li, B.; Gullappalli, H.; Pillai, V. K.; Ajayan, P. M.; Shaijumon, M. M. Electrochemical synthesis of luminescent  $\text{MoS}_2$  quantum dots. *Chem. Commun.* **2015**, 51, 6293-6296.
- 29 Ou, G.; Fan, P.; Ke, X.; Xu, Y.; Huang, K.; Wei, H.; Yu, W.; Zhang, H.; Zhong, M.; Wu, H.; Li, Y. Defective molybdenum sulfide quantum dots as highly active hydrogen evolution electrocatalysts. *Nano Res.* **2018**, 11, 751-761.
- 30 Zhang, X.; Lai, Z.; Liu, Z.; Tan, C.; Huang, Y.; Li, B.; Zhao, M.; Xie, L.; Huang, W.; Zhang, H. A facile and universal top-down method for preparation of monodisperse transition-metal dichalcogenide nanodots. *Angew. Chem.* **2015**, 54, 5425-5428.
- 31 Gopalakrishnan, D.; Damien, D.; Shaijumon, M. M.;  $\text{MoS}_2$  quantum dot-interspersed exfoliated  $\text{MoS}_2$  nanosheets. *ACS Nano.* **2014**, 8, 5297-5303.
- 32 Zhou, K.; Zhang, Y.; Xia, Z. N.; Wei, W. L. As-prepared  $\text{MoS}_2$  quantum dot as a facile fluorescent probe for long-term tracing of live cells. *Nanotechnology* **2016**, 27, 275101.
- 33 Huang, H.; Du, C. C.; Shi, H. Y.; Feng, X.; Li, J.; Tan, Y. L.; Song, W. B. Water-Soluble monolayer molybdenum disulfide quantum dots with upconversion fluorescence. *Part. Part. Syst. Character.* **2015**, 32, 72-79.
- 34 Gu, W.; Yan, Y.; Cao, X.; Zhang, C.; Ding, C.; Xian, Y. A facile and one-step ethanol-thermal synthesis of  $\text{MoS}_2$  quantum dots for two-photon fluorescence imaging. *J. Mater. Chem. B* **2016**, 4, 27-31.
- 35 Liu, T.; Chao, Y.; Gao, M.; Liang, C.; Chen, Q.; Song, G. S.; Cheng, L.; Liu, Z. Ultra-small  $\text{MoS}_2$  nanodots with rapid body clearance for photothermal cancer therapy. *Nano Res.* **2016**, 9, 3003-3017.
- 36 Zhang, P.; Xu, B.; Chen, G.; Gao, C.; Gao, M. Large-scale synthesis of nitrogen doped  $\text{MoS}_2$  quantum dots for efficient hydrogen evolution reaction. *Electrochimica Acta* **2018**, 270, 256-263.

- 37 Cai, L.; He, J.; Liu, Q.; Yao, T.; Chen, L.; Yan, W.; Hu, F.; Jiang, Y.; Zhao, Y.; Hu, T. Vacancy-induced ferromagnetism of MoS<sub>2</sub> nanosheets. *J. Am. Chem. Soc.* **2015**, 137, 2622-2627.
- 38 Zhang, X.; Qiao, X.; Shi, W.; Wu, J.; Jiang, D.; Tan, P. Phonon and Raman scattering of two-dimensional transition metal dichalcogenides from monolayer, multilayer to bulk material. *Chem. Soc. Rev.* **2015**, 44, 2757-2785.
- 39 Dong, H.; Tang, S.; Hao, Y.; Yu, H.; Dai, W.; Zhao, G.; Cao, Y.; Lu, H.; Zhang, X.; Ju, H. Fluorescent MoS<sub>2</sub> quantum dots: ultrasonic preparation, up-conversion and down-conversion bioimaging, and photodynamic therapy. *ACS Appl. Mater. Interfaces* **2016**, 8, 3107-3114.
- 40 Singh, V.; Mishra, A. K. Green and cost-effective fluorescent carbon nanoparticles for the selective and sensitive detection of iron (III) ions in aqueous solution: mechanistic insights and cell line imaging studies. *Sensors. Actuat. B-Chem.* **2016**, 227, 467-474.